Seeing Risk of Accident from In-Vehicle Cameras

Takuya Goto, Fumihiko Sakaue and Jun Sato
Nagoya Institute of Technology, Nagoya 466-8555, Japan
{goto@cv., sakaue@, junsato@}nitech.ac.jp

Keywords: Traffic Accident Prediction, Accident Risk, Risk Visualization, Instance Segmentation, Lane Detection.

Abstract: In this paper, we propose a method for visualizing the risk of car accidents in in-vehicle camera images by using deep learning. Our network predicts the future risk of car accidents and generates a risk map image that represents the degree of accident risk at each point in the image. For training our network, we need pairs of in-vehicle images and risk map images, but such datasets do not exist and are very difficult to create. In this research, we derive a method for computing the degree of the future risk of car accidents at each point in the image and use it for constructing the training dataset. By using the dataset, our network learns to generate risk map images from in-vehicle images. The efficiency of our method is tested by using real car accident images.

1 INTRODUCTION

In recent years, automated driving and driver assistance systems for automobiles have advanced rapidly, and advanced safety systems that use cameras for object recognition and collision avoidance have been developed actively. Furthermore, methods for predicting traffic accidents have also been proposed in recent years (Suzuki et al., 2018; Corcoran and Clark, 2019; Yao et al., 2019; Bao et al., 2020). However, these methods can only estimate the risk of the entire scene in the image, and they cannot map the risk for each pixel. That is, these methods cannot visualize the risk in the image.

Thus, we in this paper propose a method for estimating accident risk per pixel and generating risk map images by using deep learning. Our method takes an RGB video image as input and uses time series adversarial learning to obtain an image that represents where in the image the accident poses a danger to one's own vehicle. By using our network, the accident risk map shown in Figure 1 (b) is generated from the RGB image shown in Figure 1 (a).

However, there is no dataset in which camera images correspond to accident risk maps. In this research, we first propose a method for computing the degree of the future risk of car accidents at each point in the image and use it for constructing a training dataset that consists of pairs of in-vehicle images and risk map images. We next propose a network that generates risk map images from in-vehicle images and train it with the constructed dataset. In order to generate sequential risk map images from sequential in-vehicle camera images, we develop a network based on vid2vid (Wang et al., 2018a), a model that extends cGAN to video sequences. We combine semantic segmentation obtained from PCAN (Ke et al., 2021) and optic flow obtained from flownet2 (Ilg et al., 2017) with vid2vid for generating accurate sequential risk map images from sequential in-vehicle camera images.

(a) input image (b) risk map image (our result)

Figure 1: Accident risk map (b) estimated from in-vehicle image (a) using the proposed method.

In general, we can say that an object approaching our vehicle is dangerous, as in the case of car-to-car accidents and car-to-pedestrian accidents. However, vehicles approaching our vehicle in other lanes, such as an oncoming vehicle in another lane, pose little danger. Therefore, we in this research define a new measure of future accident risk and compute it for each point in the image.

There are many different types of in-vehicle cameras and they have different camera parameters. Thus, the degree of future accident risk must be able to be computed from images taken by cameras with different camera parameters. Therefore, we define a new measure of future accident risk so that it is invariant to the camera parameters. Then, we generate risk map

Goto, T., Sakaue, F. and Sato, J.
Seeing Risk of Accident from In-Vehicle Cameras.
DOI: 10.5220/0011743900003417
In *Proceedings of the 18th International Joint Conference on Computer Vision, Imaging and Computer Graphics Theory and Applications (VISIGRAPP 2023) - Volume 4: VISAPP*, pages 672-679
ISBN: 978-989-758-634-7; ISSN: 2184-4321

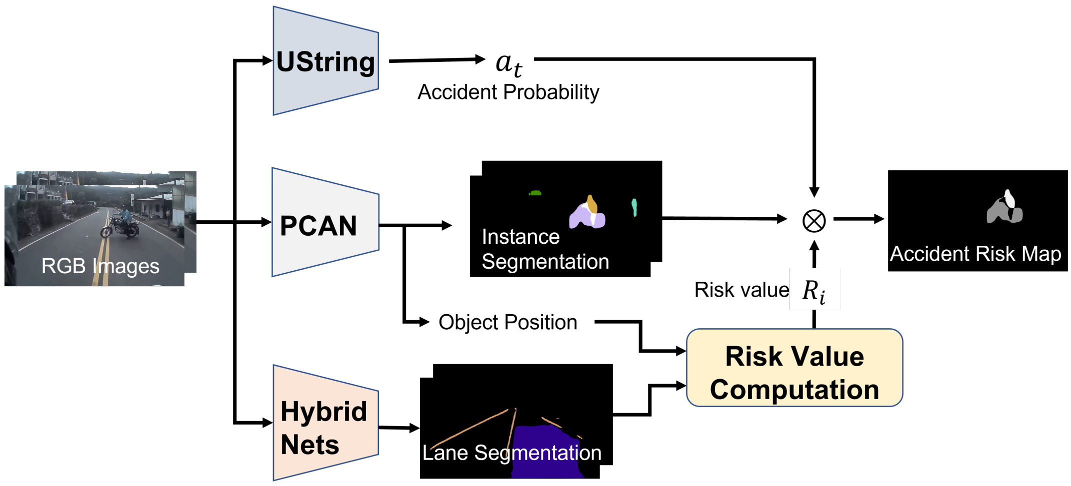

Figure 2: Dataset generation.

images that correspond to the input images by using the new risk measure and construct a training dataset using different types of cameras. By training the risk map generator by using the dataset constructed in this way, we obtain a risk map generator for various camera parameters.

2 RELATED WORK

Traffic Accident Anticipation (TAA). In order to predict traffic accidents, the existing methods estimate the likelihood of accidents occurring at each time step. DSA (Chan et al., 2016) defines candidate accident objects in each frame and uses a spatial attention mechanism for predicting traffic accidents. Based on the DSA framework, Zeng et al. (Zeng et al., 2017) realized the localization of accidents by using a soft-attention RNN. Suzuki et al. (Suzuki et al., 2018) proposed a method for early accident prediction using a quasi-recurrent neural network. Corcoran et al. (Corcoran and Clark, 2019) estimated the risk of traffic accidents using the features of candidate objects as spatial streams and optical flows as temporal streams. The two streams of information were multiplied to achieve accurate estimation. On the other hand, Yao et al. (Yao et al., 2019) proposed a method to detect anomalies on the road by predicting the future location of each object on the road. UString-Net (Bao et al., 2020) also proposes a model that takes into account the estimation of uncertainty when estimating whether an accident will occur. These methods can estimate the future risk of the entire scene from the image, but cannot map the risk for each pixel. Although (Zeng et al., 2017) realized the localization of accidents, the extracted accident has nothing to do with the observer (own vehicle), and the observer's degree of danger cannot be visualized. Differing from these existing methods, we propose a new definition of danger to observers, and propose a method to compute and map the danger for each pixel. Our method makes it possible to predict and visualize the danger to the observer, i.e. own vehicle.

Video Instance Segmentation (VIS). In our method, we use instance segmentation to compute the danger of each object in the image. The generation of an instance segmentation image from a single image contains two steps, as in Mask-RCNN (He et al., 2017). It is realized by first detecting the region of interest (RoI), then adding an object mask and dividing it into instances. Furthermore, in the case of instance segmentation in moving images, temporal mapping of each instance is realized as in Track-RCNN (Voigtlaender et al., 2019) and PCAN (Ke et al., 2021) to realize segmentation that enables tracking of the same instance in moving images. In this research, we use PCAN to perform object recognition in moving images and compute the danger of each object.

Lane Detection (LD). In our method, we perform lane detection to compute the accident risk invariant to camera parameters. The lane detection algorithm started with the Hough transform (Hassanein et al., 2015), which detects straight lines in a physics-based manner, and LaneNet (Wang et al., 2018b) used deep learning to detect individual lanes as instances. Enet-SAD (Hou et al., 2019) greatly improves the accuracy by using the Attention mechanism so that the model can self-learn. In addition to lane detection, as in Hybrid-Nets (Vu et al., 2022), we can further improve the accuracy of lane detection by segmenting the range of the roadway and multitask learning with object detection. In this research, lane detection

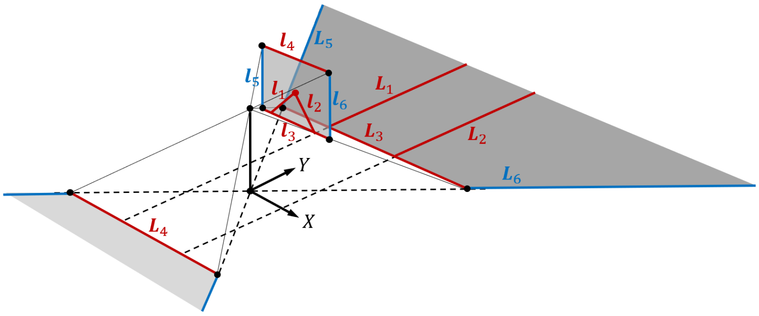

Figure 3: Projection from the image plane onto the road surface

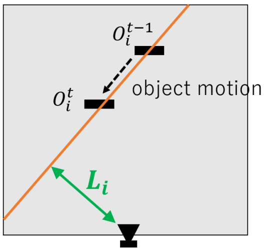

Figure 4: Distance between camera and line of object motion.

is performed using Hybrid-Nets, and the collision risk with the own vehicle is computed based on the detected lane information.

3 ACCIDENT RISK MAP DATASET

In this research, risk visualization is realized by network learning. For training our network, we need pairs of in-vehicle images and risk map images, but such datasets do not exist. Thus, in this section, we describe a method for constructing the training dataset.

3.1 Overview of Dataset Generation

Figure 2 shows the overview of our method for creating pairs of RGB images and accident risk map images. The accident risk map image is generated by multiplying the accident probability of the scene with the risk value for each segmented region in the image.

By using UString-Net (Bao et al., 2020), we can obtain the accident probability a_t in the scene. However, this is just a single value that represents the probability of an accident across the image. Thus, we multiply it with a risk map image computed from the relative position and motion between the own vehicle and each object in the image. The objects in the image are segmented and extracted by using PCAN (Ke et al., 2021). For computing the risk map image invariant to camera parameters, we also use the lane information extracted by using HybridNets (Vu et al., 2022).

We explain the detail of the risk map computation in the following sections.

3.2 Invariant Road Representation

We first extract lane markers in the image by using Hybrid-Nets (Vu et al., 2022), and obtain their line parameters $\mathbf{l}_i$ $(i = 1,2)$, i.e. homogeneous coordinates of these lines. These image lines correspond to lane markers, $\mathbf{L}_i$ $(i = 1,2)$ on the road surface. Since the lane markers are parallel to each other, their homogeneous coordinates can be represented as $\mathbf{L}_1 = [1,0,1]^\top$ and $\mathbf{L}_2 = [1,0,-1]^\top$ in the 2D projective space. We also have the line correspondence between the bottom and top image lines, $\mathbf{l}_3 = [0,1,-y_{min}]^\top$ and $\mathbf{l}_4 = [0,1,-y_{max}]^\top$, and their corresponding lines on the road surface, $\mathbf{L}_3 = [0,1,-1]^\top$ and $\mathbf{L}_4 = [0,1,1]^\top$, where y_{min} and y_{max} represent the coordinates of the bottom edge and top edge of the image. These 4 pairs of corresponding lines have the following projective relationship:

$$\mathbf{l}_i = \mathbf{H}^{-\top}\mathbf{L}_i \qquad (i = 1,\cdots,4), \tag{1}$$

and we can compute the projective transformation $\mathbf{H}$ by using these 4 pairs of lines. Once the projective transformation is obtained, we can transfer the image points $\mathbf{x}_i$ to the road surface points $\mathbf{X}_i$ as follows:

$$\mathbf{X}_i = \mathbf{H}^{-1}\mathbf{x}_i \tag{2}$$

Since the lowest point of the object region obtained by PCAN in the image is considered as a point on the road surface in the 3D space. We transfer the lowest image point of each object region to the road surface point by using the projective transformation. The derived road surface representation is invariant to camera parameters, so we can use it for computing the accident risk invariant to camera parameters.

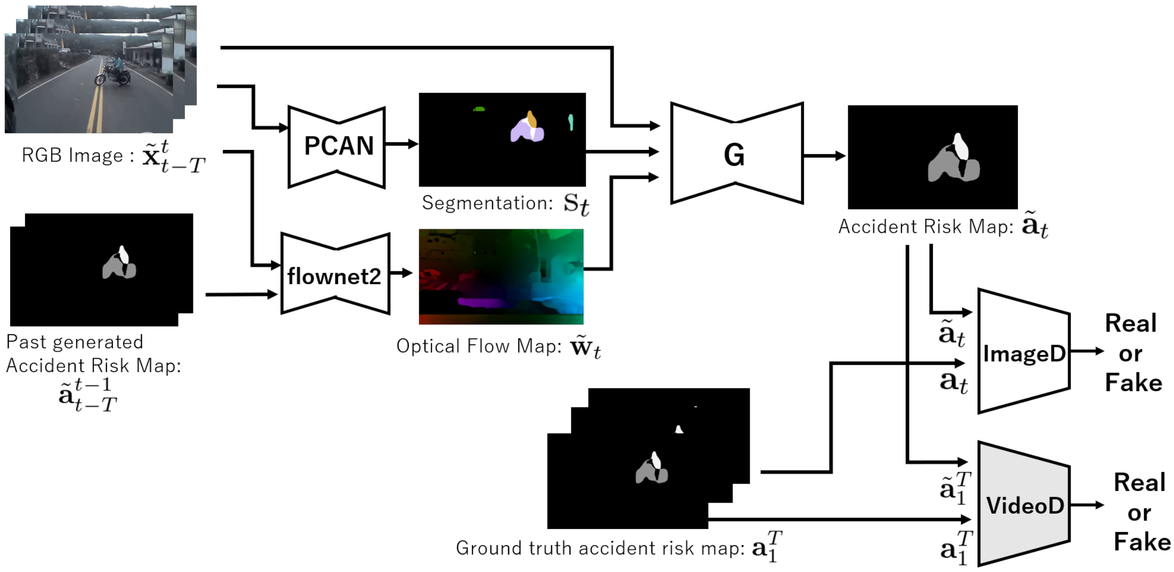

Figure 5: Proposed network for accident risk map estimation.

3.3 Computation of Accident Risk

For estimating the accident risks, we need to consider two components. The first one is distance risk and the second one is directional risk

The distance risk represents how fast the object is approaching relative to the distance to the object on the road, and it can be modeled by using Time-to-Contact (TTC) (Tresilian, 1991) as follows:

$$TTC_i = \frac{d_i^t}{d_i^t - d_i^{t-1}}, \tag{3}$$

where d_i^t is the Euclidean distance between the object i and the camera center on the road surface. Then, the distance risk P_i of object i is obtained by taking the inverse of TTC as follows:

$$P_i = \frac{1}{TTC_i} \tag{4}$$

The directional risk on the other hand represents how far the direction of motion of an object on the road is pointing in the direction of the observer. As shown in Figure 4, this can be represented by the distance L_i between the camera center and a line that represents the motion of the object O_i^t on the road. The inverse of L_i is then taken to be the directional risk D_i as follows:

$$D_i = \frac{1}{L_i} \tag{5}$$

Then, by using these two components of risk, the risk R_i of object i can be computed as follows:

$$R_i = \sigma(P_i \cdot D_i), \tag{6}$$

where, σ denotes the sigmoid function.

Then, the accident risk Q_i of the region i is computed by multiplying R_i with the accident probability across the image a_t obtained from UString-Net.

$$Q_i = a_t \cdot R_i \tag{7}$$

In this way, the accident risk at each image pixel can be computed, and we can generate an accident risk map image.

4 ESTIMATION OF ACCIDENT RISK MAPS

In Section 3, we considered a method for generating risk map images from in-vehicle images. However, this method does not work when we fail to extract lane markers in images. This situation frequently occurs around road intersections, so the method is not so practical. Thus, in this research, we use good images generated by the method described in Section 3 as training images, and realize stable risk image generation by learning the network with these training images. In our network, we also use time-series information for generating better risk map images.

Our network is based on vid2vid (Wang et al., 2018a) and uses a Markov process to capture temporal changes in images. Using the T time in-vehicle images $\mathbf{x}_1^T$ as input, T time images of accident risk map $\tilde{\mathbf{a}}_1^T$ is generated by the network. The risk map image $\tilde{\mathbf{a}}_t$ at the current time t is generated by using the past input images $\mathbf{x}_{t-L}^t$ and the risk rate map images $\tilde{\mathbf{a}}_{t-L}^{t-1}$ generated in the past as follows:

$$p\left(\tilde{\mathbf{a}}_1^T \mid \mathbf{x}_1^T\right) = \prod_{t=1}^{T} p\left(\tilde{\mathbf{a}}_t \mid \tilde{\mathbf{a}}_{t-L}^{t-1}, \mathbf{x}_{t-L}^{t}\right) \tag{8}$$

The network consists of one Generator and two Discriminators, as shown in Figure 5. Generator G takes RGB images $\mathbf{x}_{t-L}^{t}$ up to time t and risk map images generated in the past $\mathbf{a}_{t-L}^{t-1}$ as input, and generates accident risk map image at time t. It also takes segmentation images $\mathbf{s}_{t-L}^{t}$ and flow images $\mathbf{w}_{t-L}^{t}$ to further improve the accuracy. Changes of the object region are extracted by video instance segmentation, and the pixel-level temporal changes in the image are represented using optical flow derived from flownet2. Our network has two discriminators for adversarial learning. One is the image discriminator D_I, which judges whether the generated image is true or false, and the other is the video discriminator D_V, which judges whether the generated video image is natural or not. The evaluation function is as follows:

$$\min_{G}\left(\max_{D_I} \mathcal{L}_I\left(G, D_I\right) + \max_{D_V} \mathcal{L}_V\left(G, D_V\right)\right) \tag{9}$$
$$+\lambda_W \mathcal{L}_W(G) + \lambda_A \mathcal{L}_A(G),$$

where $\mathcal{L}_I$ is the adversarial loss for images as follows:

$$\mathcal{L}_I = E_{\phi_I\left(\mathbf{a}_1^T, \mathbf{x}_1^T\right)}\left[\log D_I\left(\mathbf{a}_i, \mathbf{x}_i\right)\right] \tag{10}$$
$$+E_{\phi_I\left(\tilde{\mathbf{a}}_1^T, \mathbf{x}_1^T\right)}\left[\log\left(1 - D_I\left(\tilde{\mathbf{a}}_i, \mathbf{x}_i\right)\right)\right],$$

and $\mathcal{L}_V$ is the adversarial loss for videos as follows:

$$\mathcal{L}_V = E_{\phi_V\left(\mathbf{w}_1^{T-1}, \mathbf{a}_1^T, \mathbf{x}_1^T\right)}\left[\log D_V\left(\mathbf{a}_{i-K}^{i-1}, \mathbf{w}_{i-K}^{i-2}\right)\right] \tag{11}$$
$$+E_{\phi_V\left(\mathbf{w}_1^{T-1}, \tilde{\mathbf{a}}_1^T, \mathbf{x}_1^T\right)}\left[\log\left(1 - D_V\left(\tilde{\mathbf{a}}_{i-K}^{i-1}, \mathbf{w}_{i-K}^{i-2}\right)\right)\right]$$

Also, $\mathcal{L}_w$ represents the L1 loss for the generated optical flow image as follows:

$$\mathcal{L}_W = \frac{1}{T-1}\sum_{t=1}^{T-1}\left(\|\tilde{\mathbf{w}}_t - \mathbf{w}_t\|_1\right), \tag{12}$$

and $\mathcal{L}_A$ is the L1 loss for the generated accident risk map images.

$$\mathcal{L}_A = \frac{1}{T}\sum_{t=1}^{T}\left(\|\tilde{\mathbf{a}}_t - \mathbf{a}_t\|_1\right) \tag{13}$$

By learning to minimize these losses, the network is trained to generate accident risk maps from RGB images.

5 EXPERIMENT

We next show the results of the experiments. The Dachcam Accident Dataset (DAD) (Chan et al., 2016), which is video data of real accidents, is used to create the accident risk map dataset described in Section 3. From these data, 100 types of data in which accidents have occurred and 100 types of data in which no accidents have occurred are used. For video segmentation, we used PCAN (Ke et al., 2021) trained on BDD100K dataset (Yu et al., 2018), and for lane segmentation, we used pre-trained HybridNets (Vu et al., 2022). For the true value of the optical flow, we also use the flow map estimated by using flownet2 pre-trained by the Cityscapes dataset (Cordts et al., 2016). Our network is trained using 312 video images and tested using 88 video images. We set $\lambda_W = 1.0$ and $\lambda_A = 100.0$. The generator and discriminator are trained for 200 epochs.

5.1 Dataset Creation

We first show the dataset created by using the proposed method described in Section 3.

Figure 6 shows some examples of the created dataset. We compare the data generated by the proposed method with data derived from simple Time-to-Contact (TTC) and data derived by combining TTC and directional risk without multiplying the accident probability across the image.

As shown in Figure 6, in the risk images generated from TTC only, the risk value is computed for all approaching objects, but by combining the directional risk, higher risks are assigned to the objects approaching our vehicle. However, some risks are displayed even for objects in other lanes that have no risk at all. On the contrary, the risk maps generated by the proposed method represent the risks that truly lead to accidents, as shown in the right-most column. In addition, although the angle of view and the elevation angle of these data are significantly different, the proposed method derives risk map images appropriately, and we find that the proposed method is invariant with the camera parameters.

We next show the temporal changes in the risk map images generated by the proposed method in Figure 7. For objects approaching the observer, we can see that the risk value increases as they get closer.

5.2 Estimation of Accident Risk Maps

We next show the results of our risk estimation method proposed in Section 4. The accident risk map estimated by using the network trained on the dataset generated in Section 5.1 is shown in Figure 8. In Figure 8, we show the results for two consecutive time instants for each scene. For comparison, the results derived by the existing method vid2vid are also shown.

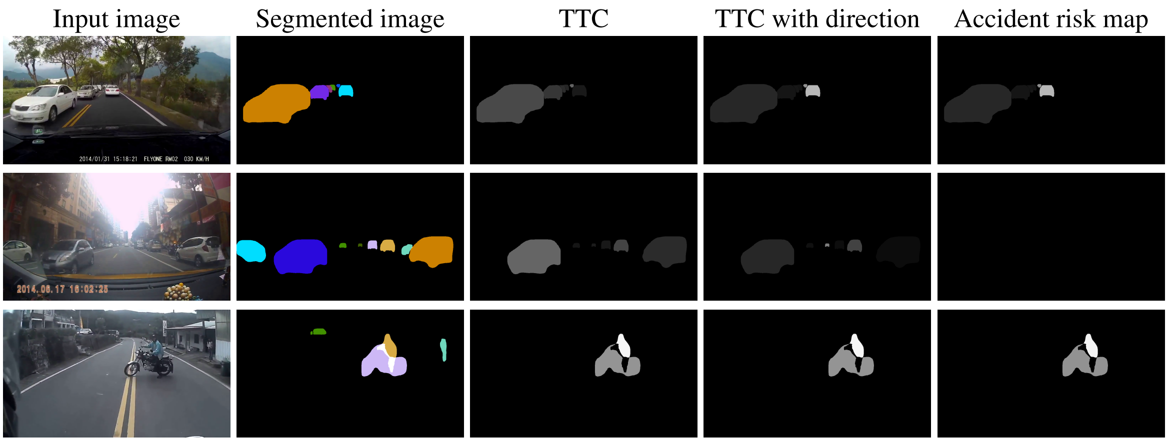

Figure 6: Dataset generated by the proposed method. first row: a scene approaching a stationary vehicle, second row: a scene without danger, third row: a scene approaching a stopped bike.

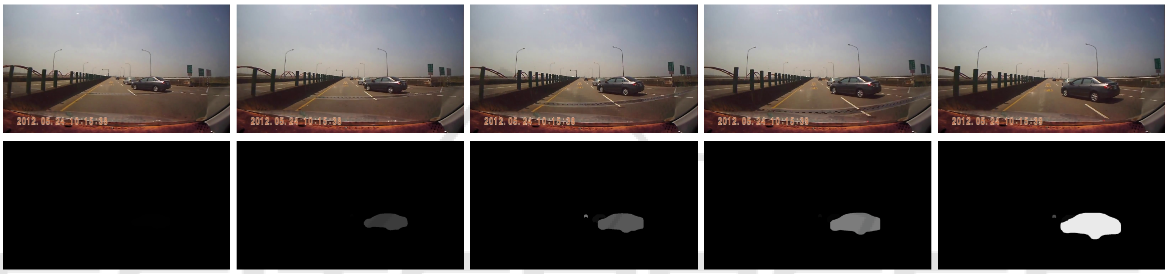

Scene 1: Vehicle is approaching from the right.

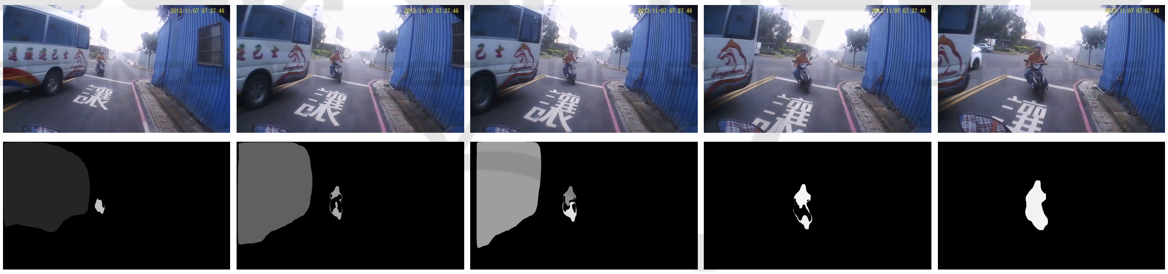

Scene 2: Bike is coming towards the observer from behind a passing bus.

Figure 7: Sequential images and their risk map images in the dataset generated by the proposed method.

Table 1: Accuracy of generated accident risk maps. To compute accuracy, precision, and recall, we binarised non-zeros to 1 and zeros to 0 in the risk value for each pixel in the generated image and computed them by taking the average of all pixels.

	RMSE	Acc	Prec	Rec
Vid2Vid	10.58	91.18	31.95	33.25
Ours (L1+gan)	9.42	94.88	56.60	58.95
Ours (L1+flow+gan)	**9.39**	**95.10**	**58.74**	**65.10**

To see the effect of flow information in the proposed method, we also compare the case where flow information is not used in the proposed method.

As shown in scene 1 in Figure 8, the risk regions derived from vid2vid are vague and not accurate, whereas the proposed method can derive the risk regions accurately. Furthermore, as shown in scene 2 and scene 3, the proposed method can estimate the risk accurately even for distant objects. We also find that combining flow information improves the accuracy of the proposed method. In scene 4, the bike was extracted accurately by adding flow information to the proposed method. The results in scene 5 also show that the risk regions derived from the existing method are vague, whereas our method can extract risk regions more accurately. However, the proposed method sometimes over-detects risk regions, so we

Figure 8: Accident risk map estimated by using the proposed network trained by using the generated dataset.

need further improvement in its accuracy.

We next show the results of the quantitative evaluation in Table 1. RMSE, Accuracy, Precision, and Recall were measured as evaluation metrics. To compute Accuracy, Precision, and Recall, we binarised non-zeros to 1 and zeros to 0 in the risk value for each pixel in the generated image and computed them by taking the average of all pixels.

While the existing method failed to correctly capture the risk regions, the proposed method was able to identify the risk regions accurately, so the proposed method improved the accuracy of RMSE and other metrics. From the values of Precision and Recall, we also find that the risks were estimated more accurately by the proposed method for regions where objects are present.

6 CONCLUSION

In this paper, we proposed a method for estimating accident risk maps, which represent the accident risk to the own vehicle, based on in-vehicle images.

The dataset required for training the GAN was created using a model independent of the camera parameters. Unlike the conventional Time-to-Contact, the dataset created by the proposed method can represent with high accuracy the greater risk only for objects approaching in the direction of the own vehicle. Moreover, by combining the trained UString-Net, it is possible to create a dataset of accident risk maps that represent only hazards in situations where accidents are likely to occur.

We also proposed a network for generating the risk map images from in-vehicle images. The proposed network trained by the proposed dataset can estimate the accident risk map more accurately than the conventional network by dealing with scenes with different camera parameters.

Finally, we confirmed through real-world experiments that the proposed method can visualize the risk to the own vehicle using any type of in-vehicle camera.

REFERENCES

Bao, W., Yu, Q., and Kong, Y. (2020). Uncertainty-based traffic accident anticipation with spatio-temporal relational learning. In *Proc. ACM International Conference on Multimedia*.

Chan, F.-H., Chen, Y.-T., Xiang, Y., and Sun, M. (2016). Anticipating accidents in dashcam videos. In *Proc. Asian Conference on Computer Vision*.

Corcoran, G.-P. and Clark, J. (2019). Traffic risk assessment: A two-stream approach using dynamic-attention. In *Proc. Conference on Computer and Robot Vision (CRV)*, pages 166–173.

Cordts, M., Omran, M., Ramos, S., Rehfeld, T., Enzweiler, M., Benenson, R., Franke, U., Roth, S., and Schiele, B. (2016). The cityscapes dataset for semantic urban scene understanding.

Hassanein, A. S., Mohammad, S., Sameer, M., and Ragab, M. E. (2015). A survey on hough transform, theory, techniques and applications. *arXiv*.

He, K., Gkioxari, G., Dollár, P., and Girshick, R. (2017). Mask R-CNN. In *Proc. International Conference on Computer Vision (ICCV)*.

Hou, Y., Ma, Z., Liu, C., and Loy, C. C. (2019). Learning lightweight lane detection cnns by self attention distillation. In *Proc. International Conference on Computer Vision*.

Ilg, E., Mayer, N., Saikia, T., Keuper, M., Dosovitskiy, A., and Brox, T. (2017). Flownet 2.0: Evolution of optical flow estimation with deep networks. In *Proc. Conference on Computer Vision and Pattern Recognition (CVPR)*.

Ke, L., Li, X., Danelljan, M., Tai, Y.-W., Tang, C.-K., and Yu, F. (2021). Prototypical cross-attention networks for multiple object tracking and segmentation. In *Proc. Advances in Neural Information Processing Systems*.

Suzuki, T., Kataoka, H., Aoki, Y., and Satoh, Y. (2018). Anticipating traffic accidents with adaptive loss and large-scale incident db. In *Proc. Conference on Computer Vision and Pattern Recognition (CVPR)*.

Tresilian, J. (1991). Empirical and theoretical issues in the perception of time to contact. *Journal of Experimental Psychology: Human Perception and Performance*, 17(3):865–876.

Voigtlaender, P., Krause, M., Osep, A., Luiten, J., Sekar, B. B. G., Geiger, A., and Leibe, B. (2019). MOTS: Multi-object tracking and segmentation. In *Proc. Conference on Computer Vision and Pattern Recognition (CVPR)*.

Vu, D., Ngo, B., and Phan, H. (2022). Hybridnets: End-to-end perception network. *arXiv*.

Wang, T.-C., Liu, M.-Y., Zhu, J.-Y., Liu, G., Tao, A., Kautz, J., and Catanzaro, B. (2018a). Video-to-video synthesis. In *Proc. Conference on Neural Information Processing Systems (NeurIPS)*.

Wang, Z., Ren, W., and Qiu, Q. (2018b). LaneNet: Real-time lane detection networks for autonomous driving. *arXiv*.

Yao, Y., Xu, M., Wang, Y., Crandall, D. J., and Atkins, E. M. (2019). Unsupervised traffic accident detection in first-person videos. In *Proc. International Conference on Intelligent Robots and Systems (IROS)*.

Yu, F., Chen, H., Wang, X., Xian, W., Chen, Y., Liu, F., Madhavan, V., and Darrell, T. (2018). Bdd100k: A diverse driving dataset for heterogeneous multitask learning. In *Proc. Conference on Computer Vision and Pattern Recognition*.

Zeng, K.-H., Chou, S.-H., Chan, F.-H., Niebles, J. C., and Sun, M. (2017). Agent-centric risk assessment: Accident anticipation and risky region localization. In *Proc. Conference on Computer Vision and Pattern Recognition (CVPR)*.